Journal of the Korean Physical Society, Vol. 49, December 2006, pp. S215∼S219

Parametric Study on Edge Localized Modes with a Coupled Peeling-Ballooning Triggering Model for the KSTAR Tokamak

Ki Min Kim, Hyun Sun Han, Ei Sung Yoon, Jin Myung Park and Sang Hee Hong*
Department of Nuclear Engineering, Seoul National University, Seoul 151-742

(Received 29 August 2005)

In order to investigate the parametric characteristics of ELMs (Edge Localized Modes) in the KSTAR (Korea Superconducting Tokamak Advanced Research) tokamak, predictive numerical simulations have been carried out by using an integrated core-edge transport modeling code. Pressure-driven ballooning modes and current-driven peeling modes are considered in a coupled form as ELM triggering mechanisms. The simulation results demonstrate that the type of triggering modes has a strong effect on the evolution of pedestal parameters such as temperature, density, and bootstrap current, due to the interferences between stabilizing or destabilizing processes of current density and pressure gradient included in the ballooning and peeling modes criteria. The evolutions of temperature and density profiles at the edge region show a mixed oscillating form of ballooning and peeling modes. The relations between pedestal parameters, such as temperature and density, and ELMs are discussed with the effects of a triggering mechanism and calculation results of pedestal parameters are presented. In addition, the maximum dumped heat fluxes onto divertor plates are given according to various pedestal conditions and heating powers.

PACS numbers: 52.55.fa
Keywords: KSTAR tokamak, Edge localized modes, Integrated simulation, Peeling-ballooning mode

I. INTRODUCTION

The H-mode as an improved confinement regime is often perturbed by the onset of quasi-periodic series of relaxation oscillations known as edge localized modes (ELMs). In particular, ELMs in the tokamak plasma cause a rapid increase of heat flux into the scrape-off layer (SOL) region and result in strong effects on divertor conditions. Hence, the pedestal parameters related to ELMs can act as constraints which impact the tokamak edge conditions to determine the global confinement [1,2]. Therefore, the control of SOL and divertor conditions is decisive to sustain stable operation of H-mode discharges, and it is essential to investigate a comprehensive understanding of the relations among ELM phenomena, pedestal parameters, and divertor heat conditions for advanced tokamak operations like H-mode discharges. In this paper, the parametric characteristics of ELMs are described with the help of numerical results obtained by an integrated core-edge transport simulation for the KSTAR (Korea Superconducting Tokamak Advanced Research) tokamak [3–5].

*E-mail: hongsh@snu.ac.kr

II. NUMERICAL MODELING

Predictive numerical simulations of ELMy H-mode discharges are carried out for the KSTAR tokamak by using an integrated plasma transport code, which has been recently developed in the authors' laboratory for a simultaneous treatment of core, edge pedestal, and scrape-off layer (SOL) regions of the tokamak [6,7]. Analytic criteria of peeling and ballooning modes are considered as ELM triggering conditions.

1. ELM models

The ELM crashes are supposed to be triggered by a current-driven peeling mode and/or a pressure-driven ballooning mode as expressed by the following criteria, respectively [8,9]:

$$\begin{aligned} &\alpha_{mhd} > \alpha_{cr}, \\ &\alpha_{mhd} \equiv -\frac{2\mu_0 R q^2}{\varepsilon B^2}\left(\frac{dp}{dr}\right), \\ &\alpha_{cr} = 0.4s\left(1+\kappa_{95}^2(1+5\delta_{95}^2)\right), \\ &\sqrt{1-4D_M} < C_k\left[1+\frac{1}{\pi q'}\oint\frac{J_{//}B}{RB_P^3}dl\right]. \end{aligned} \tag{1}$$

Table 1. KSTAR tokamak plasma parameters.

KSTAR Tokamak Parameters	
Major radius (m)	1.8
Minor radius (m)	0.5
Elongation	1.7
Triangularity	0.4
Toroidal magnetic field (T)	3.5
Plasma ions	Deuterium
Average density (m^{-3})	3.3×10^{19}

Here, $J_{||}$ is the current density parallel to the magnetic field B, and D_M is the Mercier coefficient which is proportional to the pressure gradient included in the ballooning mode criterion.

Although these models are theoretically not complete to describe accurate ELM mechanisms, they are enough to investigate the parametric characteristics of pedestal temperature, density, and SOL parameters for the ELM phenomena. In this simulation, we are only interested in the prediction of general onset conditions of ELM crashes, but the examination of the physical mechanism of ELMs is beyond the scope of this work.

2. Integrated transport modeling

The integrated transport code used in this simulation treats the core and SOL regions, respectively, with 1.5-D and 1-D approaches, which are coupled by iteration methods. In particular, the SOL model uses a simplified geometry which handles a region between the midplane and the divertor target in the direction parallel to the magnetic flux surfaces outside the separatrix for the estimation of divertor heat load [10,11].

The plasma parameters used in this simulation follow the baseline discharges of the KSTAR tokamak [12] as summarized in Table 1. In the baseline simulation, neutral beam injection (NBI) is applied as an external heating method with an 8-MW input power and plasma current is built up to 2 MA as shown in Figure 1. The temperature and density distributions of core plasma are calculated self-consistently with NBI heating profiles and SOL plasma profiles are calculated by solving multi-fluid equations.

The H-mode transition from the L-mode is assumed to occur when the released power across the separatrix exceeds the H-mode threshold power calculated by ITER database [13,14]. After the H-mode transition, transport coefficients at the edge region are reduced, exhibiting an enhanced pressure gradient at the pedestal, and maintained until pedestal parameters reach the critical values limited by ballooning and peeling criteria. At the threshold condition, the ELM crash appears and the transport coefficients at the pedestal are enhanced to 100 times the neoclassical levels at the top of the pedestal to imitate the large energy and particle losses observed at the ELM crashes.

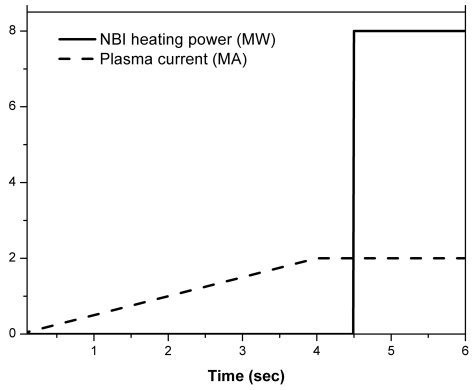

Fig. 1. NBI heating power and plasma current applied during the baseline discharges of the KSTAR tokamak.

III. SIMULATION RESULTS

1. General ELM dynamics

Pedestal density and temperature rapidly decrease by the ELM crashes and oscillate with time at a relatively constant frequency. The H-mode plasma transfers to the L-mode due to cooling of the core plasma by ELMs. However, continuous NBI heating causes re-transition to H-mode, and quasi-periodic oscillations of ELM crashes appear repeatedly.

Two different triggers, pressure-driven ballooning mode and current-driven peeling mode, cause different types of ELMs. As seen in Figure 2, the ballooning mode is more fatal to stable H-mode operations because of its faster drop of pressure, slower frequency, and larger amount of energy flux to the SOL region by one crash. On the other hand, the peeling mode crashes show more frequent oscillations and smaller temperature drops at the pedestal than the ballooning ones. Therefore, the effects of the peeling mode on tokamak confinement are relatively insignificant.

Evolutions of pedestal parameters triggered by both the ballooning and peeling modes are presented in Figure 3. The plasma density and NBI heating power have been maintained at 3.3×10^{19} m^{-3} and 4 MW, respectively. The different form of individual ELM crash is due to the coupling effect between ballooning and peeling modes. Because the growth of the pressure gradient leads a bootstrap current buildup which reduces the pressure gradient oppositely, the individual crash does not show the same fixed wave form. However, one cy-

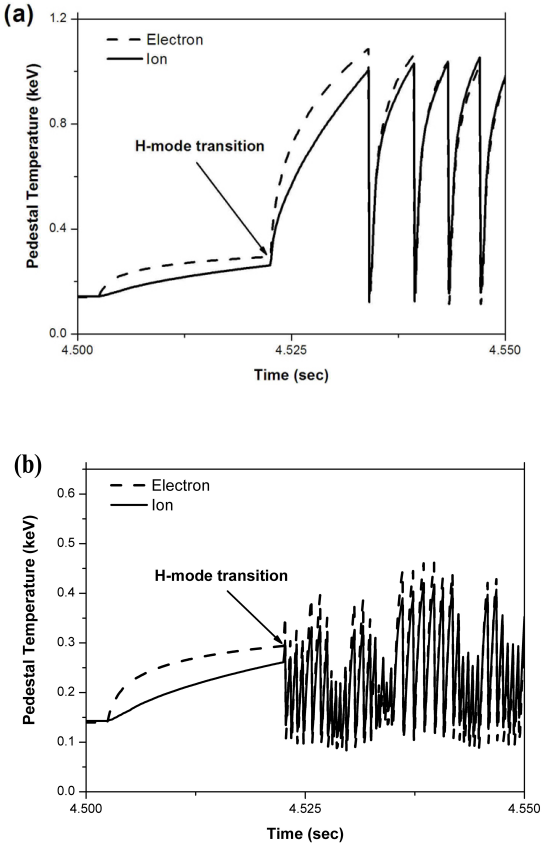

Fig. 2. Time trace of electron and ion temperature at the edge pedestal by (a) only ballooning modes, and (b) only peeling modes.

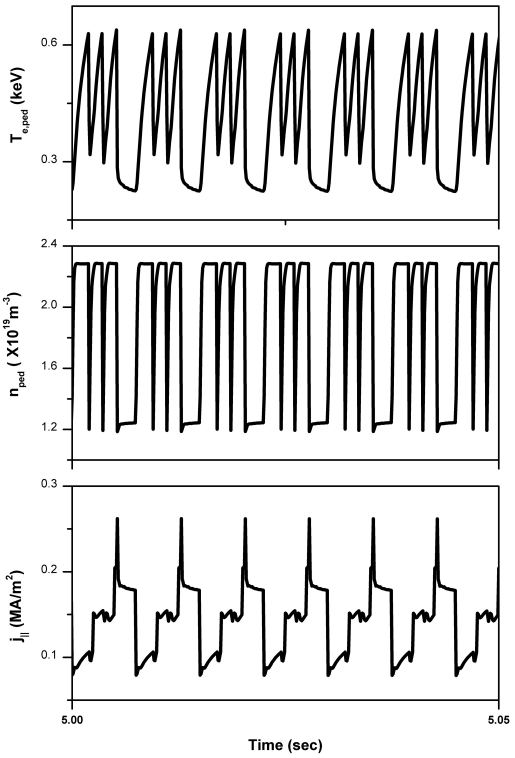

Fig. 3. Time trace of plasma temperature, density, and current density at the pedestal by peeling-ballooning modes.

cle of ELMs triggered by the coupled peeling-ballooning mode shows a similar oscillating form.

In the case of the ballooning mode, the pressure gradient increases with transport barrier formation and rapidly decreases at the critical pressure gradient, but the plasma current density does not show considerable changes. In the case of the peeling mode, the pedestal current density rapidly increases just below the critical pressure gradient due to the bootstrap current buildup by the steep pressure gradient, and moves the pedestal condition to an unstable region for the peeling mode criterion.

In the combined form of ELMs appearing in Figure 3, the ELM frequency is rather higher than that by the ballooning mode but lower than that by the peeling mode. The coupling effects between pressure and current density cause these irregularities, so more rigorous physical models seem to be required to estimate the interplay of both factors. Nevertheless, the analytic model used in the present simulation can give general information on ELM dynamics, which reflect the characteristics of ballooning and peeling modes. For instance, as the bootstrap current plays a deterministic role in increasing $J_{||}$, the increased $J_{||}$ triggers ELM crashes by making the peeling mode unstable as described in Figure 3. On the other hand, the ballooning mode is entirely dependent on the pressure gradient at the pedestal.

The ELM triggering criteria given in Section II.1. may explain such complicated temporal behaviours appearing in Figure 3. The two criteria indicate that the ballooning and peeling modes are driven by pressure gradient and parallel current density, respectively. However, the two triggering mechanisms are sophisticatedly linked, because the pressure gradient destabilizing the ballooning mode could stabilize the peeling mode on one hand by increasing its threshold value, and could destabilize the peeling mode on the other hand by inducing bootstrap currents of hollow radial distribution across the plasma column. For this reason, the ELM crashes caused by the peeling-ballooning mode show complex patterns with time.

2. Parametric characteristics of ELMs

For the parametric analysis of ELMs, numerical simulations with heating power and plasma density changed are carried out and both ballooning and peeling modes are considered as ELM triggers. First of all, the average

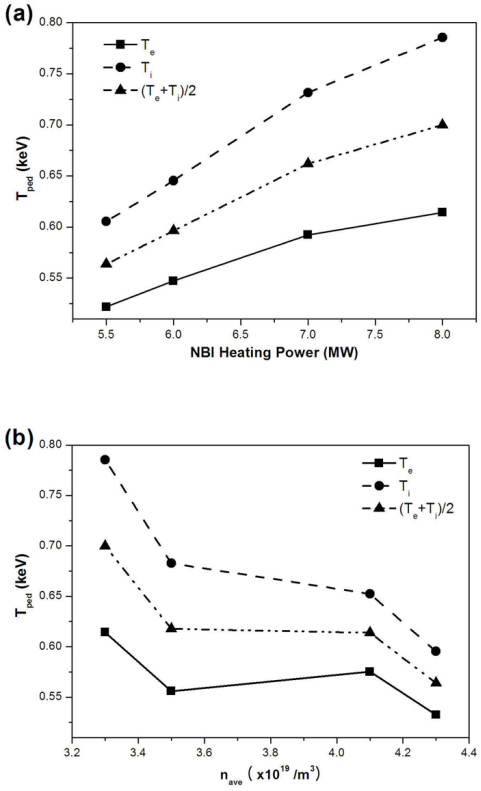

Fig. 4. Scaling of temperature of the edge pedestal with (a) NBI heating power, and (b) average plasma density.

plasma density is maintained at 3.3×10^{19} m^{-3}, and the NBI heating power increases from 5.5 MW to 8 MW. The electron and ion temperatures at the pedestal increase with heating power, and a scaling, which describes the dependency of pedestal temperature (keV) on heating power (MW), is given by the following expression:

$$\frac{T_{e,ped} + T_{i,ped}}{2} \propto P_{NBI}^{0.15} \tag{2}$$

Generally, plasma temperature is proportional to P$^{\alpha}$, where α usually falls in the range $0 \leq \alpha \leq 0.5$. The present simulation result is consistent with the experimental observations and other numerical calculations [15].

For a scaling of pedestal temperature with density, the simulation results are obtained with average plasma densities which are varied from 3.3×10^{19} m^{-3} to 4.3×10^{19} m^{-3}. 8 MW of neutral beam heating power is supplied. It is observed that the electron and ion temperatures at the top of the pedestal decrease with increasing plasma density, which reflects existing experimental results.

As a result of parametric scaling, the global dependencies of pedestal temperature on external heating power and plasma density show similar tendencies to those observed in the experimental and numerical work carried

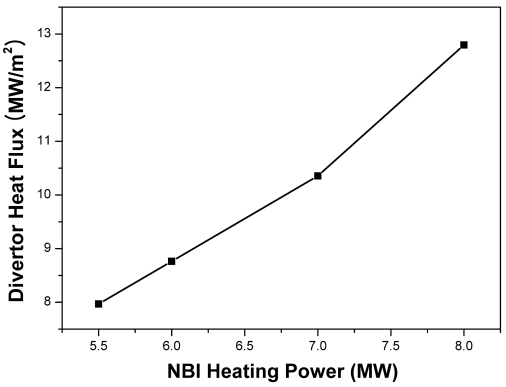

Fig. 5. Heat flux onto the divertor plate by ELM crashes, depending on NBI heating power.

out by other research groups. However, there exist some limitations of the analytic ELM criterion and the integrated transport models on the position and width of the edge pedestal. In this numerical work, the location of the pedestal is assumed to develop at the 95 % flux surface and the width of the pedestal is fixed at about 2 cm, and these assumptions could lead to some discrepancies from other results, but the overall behaviors of ELM dynamics are successfully describable to meet the purpose of this numerical work.

3. Divertor heat flux by ELMs

Since the ELM crashes triggered by both the ballooning and peeling modes accompany energy release to the SOL region, heat fluxes onto the divertor plates are rapidly increased by them and the buildup and relaxation processes are repeated, keeping pace with the pedestal parameters.

The oscillations of heat flux onto the divertor plates naturally show the same tendencies as the pedestal parameters. According to the simulation results, the maximum heat flux due to the ELM crashes exceeds about 12 MW/m^2 and increases with the neutral beam heating power, which means that the ELM crashes have intolerable effects on the divertor modules.

The dependency of divertor heat flux on heating power is given by

$$P_{Div} \propto P_{NBI}^{0.32}, \tag{3}$$

when the average plasma density has been maintained at 3.3×10^{19} m^{-3}. Divertor heat flux increases with NBI heating power as seen in Figure 5, which indicates a similar proportionality to the pedestal temperatures. As ELMs are almost unavoidable in the H-mode operation,

the powers released by ELMs to the divertor plate are expected to cause serious damage to the tokamak machine, and have influence on the confinement in the whole of the tokamak regions. From the results of this work, we can confirm that adequate controls of SOL conditions and ELMs are needed for the advanced tokamak operations targeted by the KSTAR project. The simultaneous calculations of core, edge pedestal, and SOL regions provide more reliable information for the design and operation of the tokamak machine.

IV. CONCLUSION

The numerical simulation results demonstrate that both the ballooning and peeling modes can be sources of ELMs and restrict the pedestal conditions. Especially, the evolution of edge current density, which depends on bootstrap currents and pressure gradients at the pedestal, has different effects on the pedestal parameters.

The pedestal parameters such as temperature at the top of the pedestal are seriously influenced by the operating factors related to ELMs, such as external heating power and plasma density. Moreover, the powers released by ELMs are predicted to lead to intolerable heat spikes to the target plates, which could degrade the tokamak confinement and cause a re-transition to the L-mode. For the more accurate estimation of divertor heat flux and pedestal parameters, it is required to employ an improved transport model for ELMs, including more rigorous MHD effects. An integrated transport model which considers the plasma evolution with MHD stability analysis during ELM crashes would give more reliable insights into ELM physics.

REFERENCES

[1] H. Zohm, Plasma Phys. Control. Fusion **38**, 105 (1996).
[2] J. W. Cornor, Plasma Phys. Control. Fusion **40**, 191 (1998).
[3] G. S. Lee, J. Kim, S. M. Hwang, C. S. Chang, H. Y. Chang, M. H. Cho, B. H. Choi, K. Kim and K. W. Cho, *et al.*, Nucl. Fusion **40**, 575 (2000).
[4] Keeman Kim, H. K. Park, K. R. Park, B. S Lim, S. I. Lee, M. K. Kim, Y. Chu, W. H. Chung and S. H. Baek, *et al.*, J. Korean Phys. Soc. **44**, 1195 (2004).
[5] J. S. Yoon, Y. D. Bae, J. G. Kwak and B. G. Hong, J. Korean Phys. Soc. **44**, 1203 (2004)
[6] J. M. Park, S. H. Kim, K. M. Kim and S. H. Hong, Bullet. Am. Phys. Soc. **48**, 346 (2003).
[7] S. H. Kim, J. M. Park and S. H. Hong, J. Korean Phys. Soc. **46**, 861 (2005).
[8] H. R. Wilson, J. W. Connor, A. R. Field, S. J. Fielding, R. J. Hastie, R. L. Millera and J. B. Taylor, Nucl. Fusion **40**, 713 (2000).
[9] J. S. Lönnroth, V. Parail, A. Dnestrovskij, C. Figarella, X. Garbet, H. Wilson and JET-EFDA Contributors, Plasma Phys. Control. Fusion **46**, 1197 (2004).
[10] S. Nakazawa, N. Nakajima, M. Okamoto and N. Ohyabu, Plasma Phys. Control. Fusion **42**, 401 (2000)
[11] D. K. Kim and S. H. Hong, Phys. Plasma **12**, 062504 (2005).
[12] J. S. Ko, D. K. Kim, S. H. Hong and K. H. Im, J. Korean Phys. Soc. **41**, 212 (2002).
[13] Y. Shimomura, Y. Murakami, A. R. Polevoi, P. Barabaschi, V. Mukhovatov and M. Shimada, Plasma Phys. Control. Fusion **43**, A385 (2001)
[14] Yong-Su Na, J. Korean Phys. Soc. **48**, 576 (2006).
[15] A. Y. Pankin, I. Voitsekhovitch, G. Bateman, A. Dnestrovski, G. Janeschitz, M. Murakami, T. Osborne, A. H. Kritz, T. Onjun, G. W. Pacher and H. D. Pacher, Plasma Phys. Control. Fusion **47**, 483 (2005).